Hindawi
International Journal of Antennas and Propagation
Volume 2017, Article ID 3049532, 11 pages
https://doi.org/10.1155/2017/3049532

Research Article

Modelling of Electromagnetic Scattering by a Hypersonic Cone-Like Body in Near Space

Ji-Wei Qian,[1] Hai-Li Zhang,[2] and Ming-Yao Xia[1]

[1]*School of Electronics Engineering and Computer Science, Peking University, Beijing 100871, China*
[2]*School of Electronic Engineering, University of Electronic Science and Technology of China, Chengdu 611731, China*

Correspondence should be addressed to Ming-Yao Xia; myxia@pku.edu.cn

Received 9 October 2016; Revised 30 November 2016; Accepted 15 January 2017; Published 7 February 2017

Academic Editor: Atsushi Mase

A numerical procedure for analysis of electromagnetic scattering by a hypersonic cone-like body flying in the near space is presented. First, the fluid dynamics equation is numerically solved to obtain the electron density, colliding frequency, and the air temperature around the body. They are used to calculate the complex relative dielectric constants of the plasma sheath. Then the volume-surface integral equation method is adopted to analyze the scattering properties of the body plus the plasma sheath. The Backscattering Radar Cross-Sections (BRCS) for the body flying at different speeds, attack angles, and elevations are examined. Numerical results show that the BRCS at a frequency higher than 300 MHz is only slightly affected if the speed is smaller than 7 Mach. The BRCS at 1 GHz would be significantly reduced if the speed is greater than 7 Mach and is continuously increased, which can be attributed to the absorption by the lossy plasma sheath. Typically, the BRCS is influenced by 5~10 dBm for a change of attack angle within 0~15 degrees, or for a change of elevation within 30~70 km above the ground.

1. Introduction

In addition to the conventional reentries, more and more hypersonic bodies are emerging in the near space in recent years. Finding, tracking, and identification of these kinds of targets are of great importance for both civil and military purposes. Analysis of scattering properties of these bodies constitutes an essential part to achieve the goals. Compared with the analysis of scattering by motionless or low-speed targets, a great challenge comes from simulating the formation of the plasma sheath when the target is flying at hypervelocity in the near space, for which solving the fluid dynamics equations would be a premise. The plasma sheath should be considered as an extended part of the body. Another challenge involves the electrical large size issue, for which the number of unknowns can be more than one million. For the present problem, the domain under study consists of the perfectly conducting body itself plus the inhomogeneous plasma medium. Heterogeneity of the target and the plasma sheath adds the handling complexity.

Research on the electromagnetic scattering by or propagation through high temperature and high speed air or plasma medium may be dated back to the end of the 1950s [1–3]. Extensive investigations on the topic were continued in the 1960s [4–14]. Formation of plasma wake or sheath due to a hypersonic vehicle was studied in [4, 5]. Analysis of scattering by the plasma wakes by means of asymptotical expansion with the stationary phase method, as well as the approximate Wentzel-Kramers-Brillouin (WKB) method, were carried out by many authors [3, 6–8]. Scattering properties of an infinite metal cylinder covered with inhomogeneous and anisotropic plasma sheath under the parabolic electron density profile assumption were investigated and reported in [9–12]. Propagation problems of electromagnetic (EM) waves in the plasma sheath created by a hypersonic vehicle were discussed in [2, 13, 14]. Recently, Dutta et al. revisited the EM propagation in the plasma sheath and proposed a scheme for mitigation of RF blackout [15]. These works were largely qualitative due to the restriction of computing ability in the ages.

With the advents of high-performance computers and high efficient algorithms, numerical techniques were devised to solve the Navier-Stokes equation and the Maxwell equations, giving birth to the computational fluid dynamics (CFD) and the computational electromagnetics (CEM). Now, useful

CFD tool kit such as the CFD-Fastran is available to simulate the generation of the plasma sheath due to a hypersonic vehicle. In regard to the CEM methods for analysis of scattering by combined conductor with dielectric/plasma medium, a range of approaches were developed, including the finite difference time domain (FDTD) method [16–19], the finite element method (FEM) [20], and the integral equation based method of moments (MoM) [21–23]. A multilayered thin dielectric sheet (ML-TDS) approximation method was also presented to deal with the plasma sheath scattering problem [24, 25]. However, the distributions of plasma sheath in these papers were assumed, because experiment or simulation data of the plasma sheath was hardly available.

The purpose of the present work is to develop a relatively rigorous procedure to extract the scattering characteristics of a hypersonic object flying in the near space. The meaning of rigorousness is twofold: (i) the data of plasma sheath for a hypersonic cone-like body is obtained by numerically solving the Navier-Stokes equation under some appropriate conditions, rather than being assigned by assumptions, and (ii) the analysis of scattering is based on reliable computational electromagnetics methods, rather than based on approximate analytical evaluations.

2. Method

2.1. Modeling of Plasma Sheath. When a hypersonic object flies at an extremely high speed, the air around the object is compressed quickly, which produces the flow fields. Collisions between molecules in the flow fields are greatly enhanced due to the high density of the compressed air, which generate a large amount of heat that ionizes the air. The components of air react with each other under the rules of chemical reactions with the help of high temperature, and a kind of inhomogeneous medium that we call the plasma sheath is formed and covers the object. So modeling of the plasma sheath is an essential step for analysis of scattering by hypersonic objects flying in the near space. The modeling would involve three aspects: flow field control model, temperature model, and chemical reaction model.

In regarding to the flow field control model, according to the hydromechanics theory, the flow fields around the object should satisfy the Navier-Stokes (NS) control equation with the condition of chemical nonequilibrium [26]. The NS equation accounts for the basic laws, including the mass, momentum, and energy conservations.

As for the temperature model which describes the thermal state of the physical process, conventional single temperature model which assumes that the translational temperature, rotational temperature, and vibrational temperature are all the same, could not correctly explain the changes of the molecular internal energy. The triple-temperature model is an accurate way to solve the problem, but the computing burden is very heavy. As a compromise, we adopt the Park double temperature model [27], in which one temperature T describes the translational energy and rotational energy of the particles, and the other temperature T_v describes the vibrational energy and the electron energy of the particles.

Table 1: The chemical reactions in seven species model.

Number	Chemical reaction
1	$N_2 + M \rightleftharpoons N + N + M$
2	$O_2 + M \rightleftharpoons O + O + M$
3	$N_2 + O \rightleftharpoons NO + N$
4	$NO + M \rightleftharpoons O + N + M$
5	$NO + O \rightleftharpoons N + O_2$
6	$N_2 + N \rightleftharpoons 2N + N$
7	$N + O \rightleftharpoons NO^+ + e^-$

The chemical reaction model is the key to produce the plasma sheath with the rising of temperature. The air is a kind of mixture which contains many kinds of gas. To simplify the problem, we assume that the air contains seven species, including N_2, N, O_2, O, NO, NO^+, and e^-. They react with each other and finally form the plasma sheath. The chemical reactions of the seven species and the seven reactions model are adopted in the present work as shown in Table 1, in which M represents the colliding molecules, including N_2, N, O_2, O, and NO [28].

Description of computational methods for the flow fields in great detail is complex and not essential and is omitted here, which may be reported elsewhere. Once the flow fields around the object are resolved, the gas temperature $T(\mathbf{r})$ and electron density $n_e(\mathbf{r})$ are obtained. The ionized gas may be taken to be isotropic unmagnetized plasma ($\mu_r = 1$). According to the Boltzmann equation, the complex relative dielectric constant of the plasma can be expressed as [29]

$$\varepsilon_r = \left(1 - \frac{\omega_p^2}{\omega^2 + \nu^2}\right) - j\frac{\nu}{\omega}\frac{\omega_p^2}{\omega^2 + \nu^2} \tag{1}$$

with

$$\omega_p^2(\mathbf{r}) = n_e(\mathbf{r})\frac{e^2}{m_e\varepsilon_0}, \qquad \nu(\mathbf{r}) = 5.2 \times 10^{13} n_e(\mathbf{r})\left[\kappa T(\mathbf{r})\right], \tag{2}$$

where ω_p is the plasma angular frequency, $\kappa = 1.38 \times 10^{-23}$ is the Boltzmann constant, $\nu(\mathbf{r})$ is the average collision frequency of electrons with molecules, and the other symbols have their common senses.

2.2. Analysis Method for Scattering. The hypersonic object is supposed to be a perfect electrical conductor (PEC) shaded by the plasma sheath. The incident wave would induce a distribution of surface current $\mathbf{J}_S$ on the object surface S and a distribution of equivalent volume current $\mathbf{J}_V$ within the plasma domain V. The total scattered field produced by the surface currents and volume currents are expressed as

$$\mathbf{E}^s = -\eta_0 \mathscr{L}(\mathbf{J}_S) - \eta_0 \mathscr{L}(\mathbf{J}_V), \tag{3}$$

$$\mathbf{H}^s = -\mathscr{K}(\mathbf{J}_S) - \mathscr{K}(\mathbf{J}_V) \tag{4}$$

with $\eta_0 = \sqrt{\mu_0/\varepsilon_0}$ and

$$\mathscr{L}(\mathbf{J}_S) = jk \int_S \overline{\mathbf{G}}(R) \cdot \mathbf{J}_S(\mathbf{r}')\, dS',$$
$$\mathscr{K}(\mathbf{J}_S) = \int_S \mathbf{J}_S(\mathbf{r}') \times \nabla G(R)\, dS', \quad (5)$$
$$\overline{\mathbf{G}}(R) = \left(\overline{\mathbf{I}} + \frac{1}{k^2}\nabla\nabla\right) G(R), \quad G(R) = \frac{e^{-jkR}}{4\pi R},$$

where $G(R)$ is the scalar Green's function and $\overline{\mathbf{G}}(R)$ is the dyadic Green's function. The operators of $\mathscr{L}(\mathbf{J}_V)$ and $\mathscr{K}(\mathbf{J}_V)$ are similar, just replacing the integral over the object surface by the integral within the plasma region.

On the object surface, the electric field and magnetic field must satisfy the boundary conditions

$$\hat{n} \times \left(\mathbf{E}^i + \mathbf{E}^s\right) = 0,$$
$$\hat{n} \times \left(\mathbf{H}^i + \mathbf{H}^s\right) = \mathbf{J}_S. \quad (6)$$

By combining these two equations, we obtain the Combined Field Integral Equation (CFIE)

$$-\alpha \frac{1}{\eta_0} \hat{n} \times \hat{n} \times \mathbf{E}^s + (1-\alpha)\left(\mathbf{J}_S - \hat{n} \times \mathbf{H}^s\right)$$
$$= \alpha \frac{1}{\eta_0} \hat{n} \times \hat{n} \times \mathbf{E}^i + (1-\alpha)\, \hat{n} \times \mathbf{H}^i, \quad (7)$$

where α is a factor satisfying $0 \le \alpha \le 1$. Within the plasma domain, the equivalent volume current is related to the total electric field by $\mathbf{J}_V = j\omega\varepsilon_0(\varepsilon_r - 1)\mathbf{E}$, or

$$\mathbf{J}_V - j\omega\varepsilon_0\left(\varepsilon_r - 1\right)\mathbf{E}^s = j\omega\varepsilon_0\left(\varepsilon_r - 1\right)\mathbf{E}^i. \quad (8)$$

By substituting (3)~(5) into (7) and (8), a set of coupled Volume-Surface Integral Equations (VSIE) to be solved for $\mathbf{J}_S$ and $\mathbf{J}_V$ is constructed.

The VSIE methods presented in [21, 22] are employed to solve the set of equations. Once the currents are solved out, the scattered fields can be calculated by (3). Particularly, we are concerned with evaluating the influences of the plasma sheath on the Backscattering Radar Cross-Section (BRCS).

3. Simulation Results

In this section, a wealth of simulations are performed to examine the influences of some factors on the morphological feature or pattern of the plasma sheath and its electromagnetic scattering properties. The factors include the velocity, attack angle, and flight height. The computing platform is a high-performance Dell server with 40 processors and 512 GB core memory. Simulation steps are exemplified by using a PEC cone-like body as the hypersonic object. The height of the object is 112.5 cm, and the diameter of its base is 42 cm. The model and sizes are shown in Figure 1.

3.1. Meshing for CFD and CEM Simulations. In order to solve the problem through numerical methods, appropriately meshing the object surface and plasma domain is essential. However, the meshes for the computational fluid dynamics (CFD) and computational electromagnetics (CEM) are not consistent.

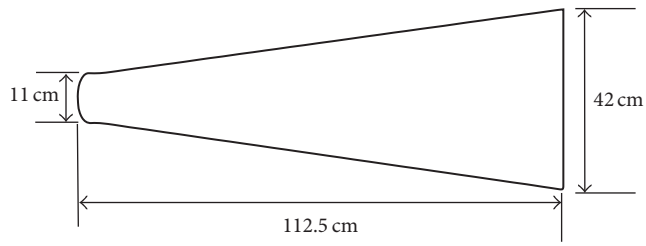

Figure 1: The cone-like object for study.

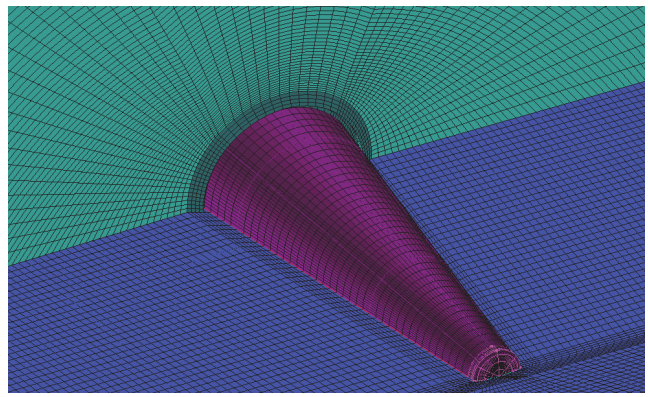

Figure 2: Meshing for analysis of flow fields. Green represents the meshes of the plasma domain in a plane perpendicular to the object axis; blue represents the meshes in the symmetry plane; and purple represents the conformal meshes on the object surface.

For the simulation of CFD, the computational domain around the object is taken to be about several times larger than the object itself. Here a cylindrical domain with a height of 342 cm and a diameter of 300 cm is used to analyze the flow fields. There are two points that we need to consider. First, hexahedral discretization should be adopted, which is a kind of irregular grid to meet the requirement of chemical reactions in the CFD solver. The irregular hexahedron grids should also be conformal with the object surface. Second, because the flow fields change sharply near the object surface and slowly far away from the object, the meshes must be sufficiently dense near the object and sparse far away. Due to the symmetry of the calculated domain, only half region is needed to be solved for. As a result, a total of 610,151 hexahedral cells have been generated. The meshing for flow field simulation is shown in Figure 2.

As for the simulation of CEM, the computational domain is the same as that of the flow field analysis. The whole domain is discretized by using tetrahedral cells and the complex relative dielectric constant in each cell is calculated. Those cells whose dielectric constants are very close to that of the air (i.e., $|\varepsilon_r - 1| < 10^{-4}$) will not be seen as plasma cells. As a result, though the total amount of tetrahedral cells is very large, the number of efficient plasma cells is only

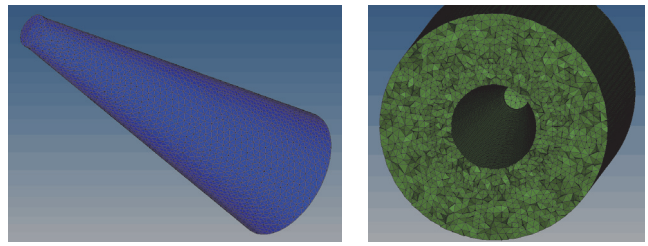

(a) (b)

Figure 3: Meshing for analysis of scattering. (a) Triangulation of the object surface and (b) tetrahedralization of the plasma domain.

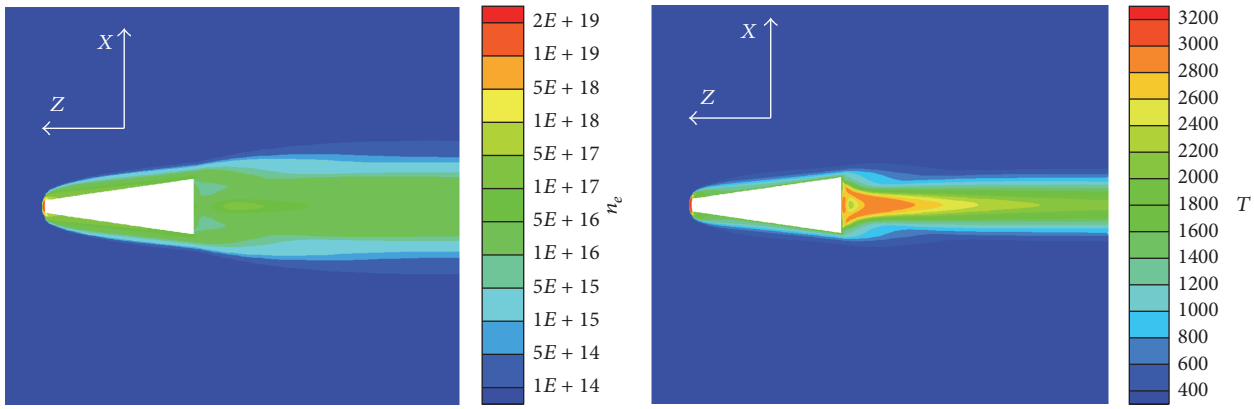

(a) (b)

Figure 4: The distributions of electron density and gas temperature of the plasma sheath for the object flying at 8 Mach, null attack angle, and 30 km above the ground. (a) The electron density and (b) the gas temperature.

393,199, which results in a total of 786,398 unknowns by using the Schaubert-Wilton-Glisson (SWG) basis functions [30]. The object surface is discretized with 5,646 triangular patches, which generates 8,469 unknowns by using the Rao-Wilton-Glisson (RWG) basis functions [31]. The meshing for scattering simulation is shown in Figure 3.

Because the meshes for the CEM and CFD simulations are different, an averaging scheme is used to calculate the complex relative dielectric constant in a CEM cell by using the data in the CFD cells:

$$\varepsilon_r\left(\mathbf{r} \in V_n\right) = \frac{1}{M}\sum_{m=1}^{M} \varepsilon_r\left(\mathbf{r}_m\right), \tag{9}$$

in which V_n is nth tetrahedral cell for CEM and $\mathbf{r}_m$ is the mth point within or near V_n where the CFD data are recorded. M in (9) varies with position. Near the object surface, where the CFD cell size is much smaller than the CEM cell size, M may be greater than 60. Far away from the object surface, where the CFD cell size could be greater than the CEM cell size, averaging over several nearby cells would be used; that is, M is taken to be the number of CFD cells around the CEM cell, which is about 8.

3.2. Pattern of Plasma Sheath. In this subsection, the morphological features of the plasma domain are investigated by changing the flight parameters, including the velocity, attack angle, and flight height.

First, a typical distribution for the electron density and a typical distribution for the gas temperature are shown in Figure 4. The velocity, attack angle, and flight height are taken to be 8 Mach, zero degrees, and 30 km above the ground, respectively. The highest electron density and the highest gas temperature are located near the object head, reaching about $10^{19}/\mathrm{m}^3$ and 3200 K, respectively. Due to the unavailability of real plasma data around the object, checking the accuracy of the simulation results is not practical. However, some qualitative comparison may be made with the measured data in the 1960s [32]. In the experiment, a cone object is flying at 22 Mach and 70 km above the ground. The electron density at a position that is 1.84 cm away from the surface of rear part of the object is measured to be about $3 * 10^{17}/\mathrm{m}^3$. Our simulation results show that at the same height of 70 km, for the speeds at 10 Mach and 15 Mach, the electron density at the corresponding position is about $8 * 10^{16}/\mathrm{m}^3$ and $2 * 10^{17}/\mathrm{m}^3$, respectively. We fail to obtain the simulation data for 22 Mach because of insufficient computing resources. Considering the increasing tendency of the electron density with the speed and the difference of our object model with the experiment model, we may think that our simulation results are trustful.

By using (1)-(2), the complex relative dielectric constant can be calculated, which are shown in Figure 5, where the incident wave frequency has been taken to be 1 GHz. It is seen

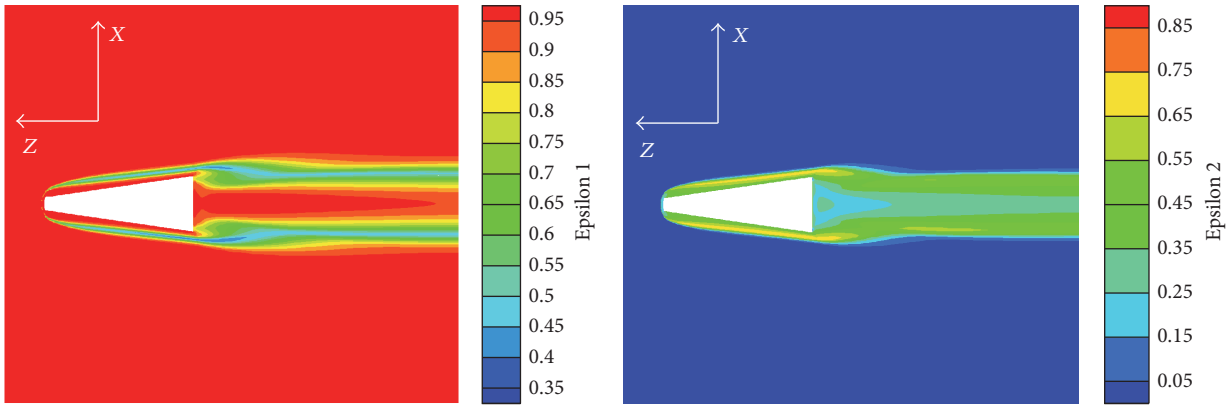

(a) (b)

FIGURE 5: The complex relative dielectric constant of the plasma sheath for the object flying at 8 Mach, null attack angle, and 30 km above the ground. (a) The real part and (b) the imaginary part.

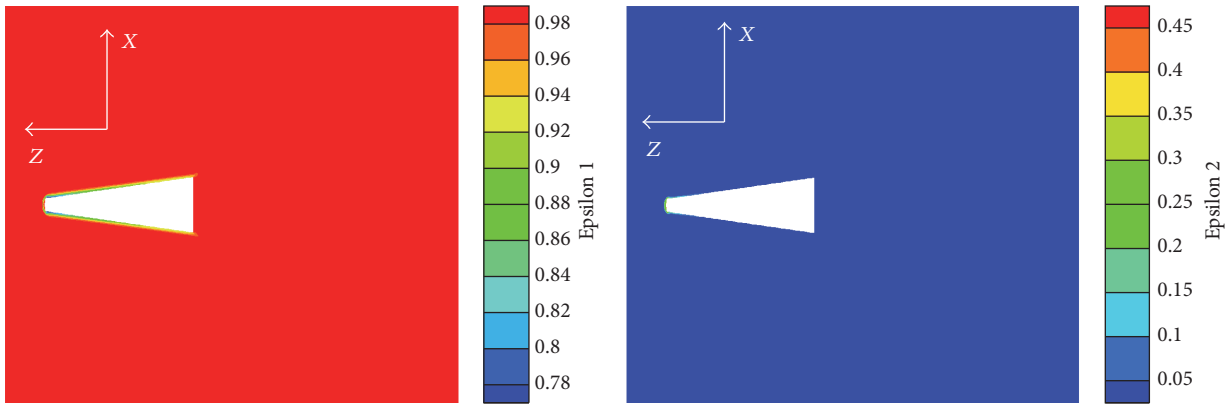

(a) (b)

FIGURE 6: The complex relative dielectric constant of the plasma sheath for the object flying at 7 Mach, null attack angle, and 30 km above the ground. (a) The real part and (b) the imaginary part.

that the real part is between 0.35 and 1, and the imaginary part is between 0.05 and 0.85. Also, the plasma domain looks quite broad. From these morphological features, we may infer that if the object flies at 8 Mach and 30 km above the ground, the plasma sheath effects on scattering properties at the EM wave frequency 1 GHz would be significant.

To reveal how the velocity affects the formation of the plasma sheath, the velocity is decreased from 8 Mach to 7 Mach. It is found that electron density at 7 Mach would be decreased by two orders of magnitude smaller than that at 8 Mach. The results of the complex relative dielectric constant at 1 GHz are shown in Figure 6. It looks obvious that though the minimum value of the real part and the maximum value of the imaginary part reach 0.78 and 0.4, respectively, the plasma sheath is formed only within a very small region near the object head and surface. In this case, the impact of the plasma sheath on the scattering properties should be very slight. As a result, we may conclude that the velocity from 7 Mach to 8 Mach is a transition region for the plasma sheath to become prominent, if the incident EM wave frequency is greater than 1 GHz.

To proceed with, the velocity is increased to 10 Mach. The results of the complex relative dielectric constant are shown in Figure 7. Compared with Figure 5, obvious changes of both the real part and imaginary part are observed. It appears that they are compressed to become thinner. The minimum value of the real part and the maximum value of the imaginary part reach −0.2 and 1.9, respectively. If the velocity is continuously increased, the plasma sheath would look thinner and thinner until little change would be observed, which may be understood that the gas molecules have been sufficiently ionized.

Now, we consider the change of attack angle. The results of the real parts of the complex relative dielectric constants are shown in Figure 8, as the attack angle is increased from zero degrees to 15 degrees. The velocity and flight height are taken to be 10 Mach and 50 km above the ground, respectively. It is apparent that though the range of values of the relative dielectric constants is almost the same, the patterns of the plasma sheath are changed greatly. Accordingly, the scattering properties would be changed appreciably.

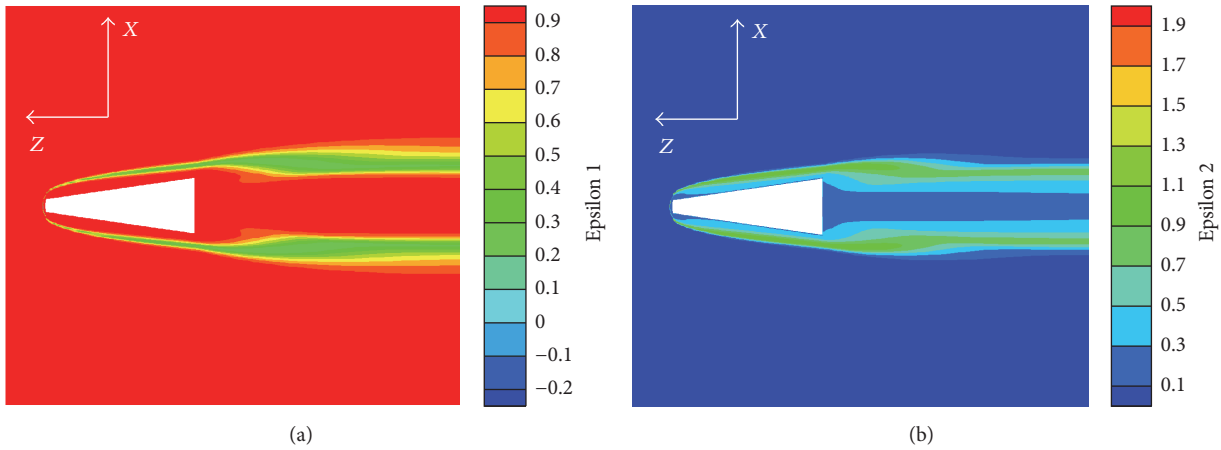

FIGURE 7: The complex relative dielectric constant of the plasma sheath for the object flying at 10 Mach, null attack angle, and 30 km above the ground. (a) The real part and (b) the imaginary part.

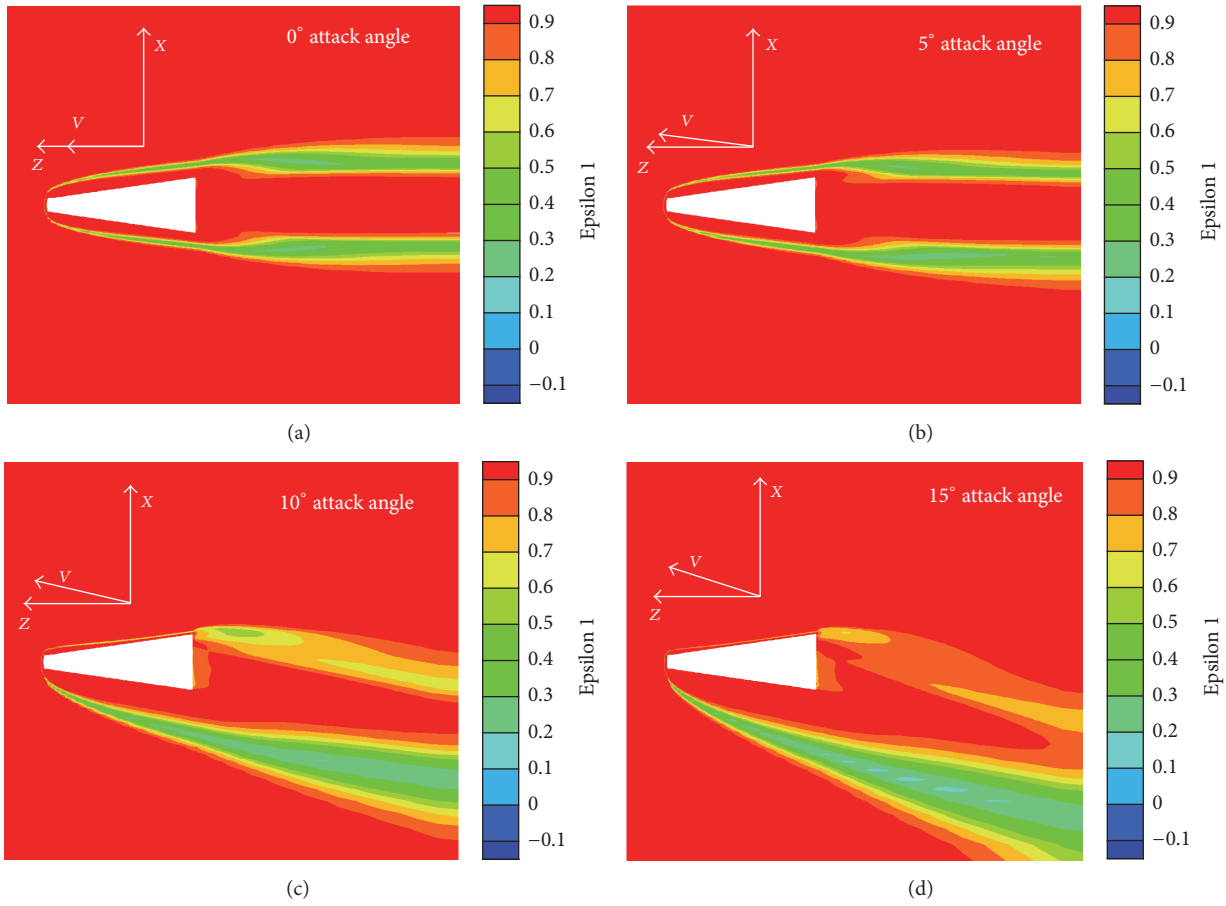

FIGURE 8: The real parts of the complex relative dielectric constant of the plasma sheath for the object flying at different attack angles. The velocity and height are 10 Mach and 50 km above the ground, respectively. (a) At null attack angle; (b) at 5-degree attack angle; (c) at 10-degree attack angle; and (d) at 15-degree attack angle.

Finally, the morphological features of the plasma sheath for the object flying at different heights are studied. Because the components, pressure, and temperature of the air are changing at different height, the dielectric parameters of the formed plasma sheath might change a lot. However, numerical results show that the changes are not as prominent as we thought, as shown in Figure 9 for the object flying at 30 km, 50 km, and 70 km above the ground, respectively. The velocity and attack angle have been assumed to be 10 Mach and zero degrees, respectively. If the flight height is

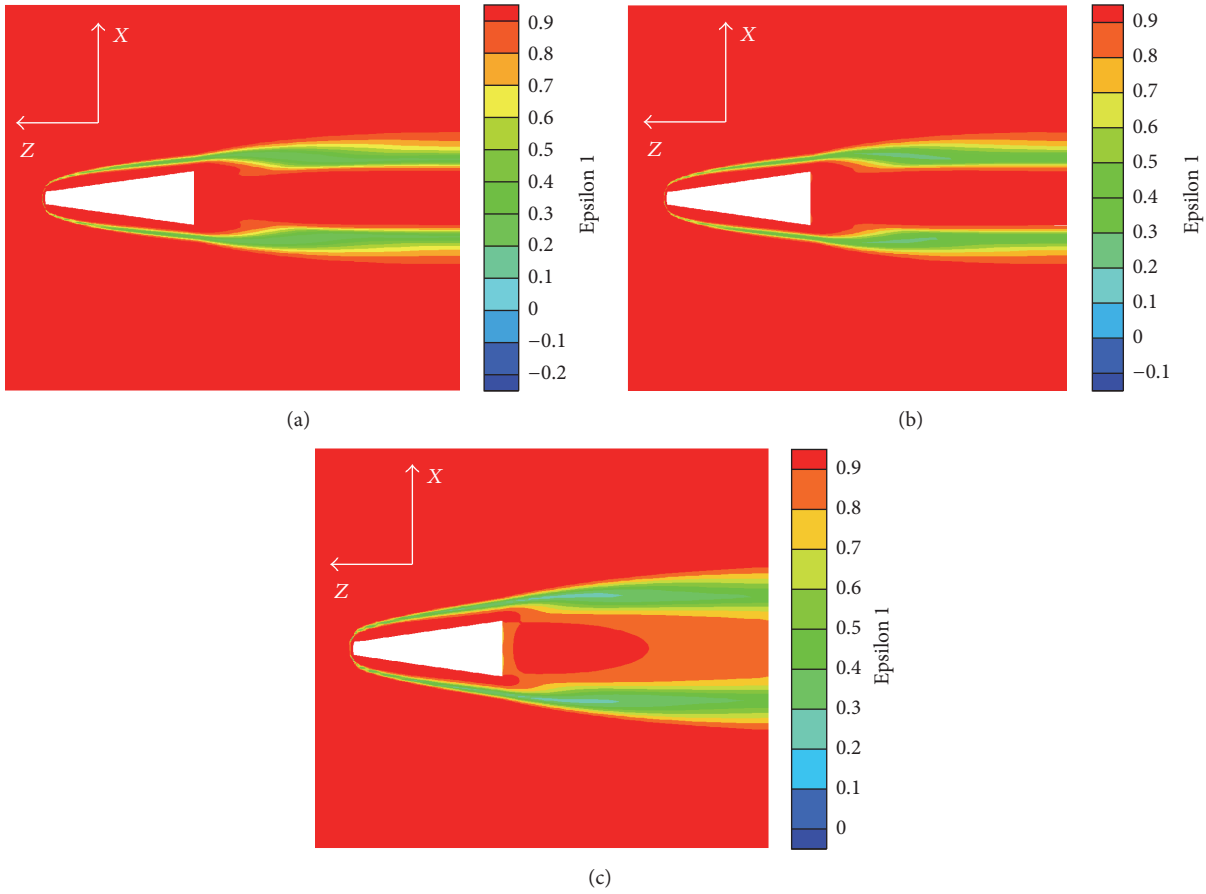

FIGURE 9: The real parts of the complex relative dielectric constant of the plasma sheath for the object flying at different height above the ground. The velocity and attack angle are taken to be 10 Mach and zero degrees, respectively. (a) At 30 km; (b) at 50 km; and (c) at 70 km.

continuously increased, one may imagine that the plasma sheath effect would become weaker and weaker, as the air becomes rarer and rarer.

3.3. Analyses of Scattering Properties. In this subsection, the influences of the plasma sheath on the Backscattering Radar Cross-Section (BRCS) are examined under different flying states.

First, for the object flying at null attack angle and 30 km above the ground, comparisons of the BRCS for a set of velocities are shown in Figure 10, where the frequency of incident waves is $f = 1$ GHz. It can be seen that if the velocity is smaller than 7 Mach, the influences are very slight for both copolarizations. Significant changes take place when the velocity is increased from 7 Mach to 8 Mach. In general, the BRCS are reduced in almost all directions. This may be accounted for the fact that the plasma sheath has absorbed some energy from the incident waves. As the velocity is increased to 10 Mach, the BRCS are reduced in most directions but could be enhanced in some directions. This seems to imply that the total amount of absorbed energy is approaching a steady level.

In view that, according to (1), as the incident wave frequency decreases, the real part and the imaginary part of the complex relative dielectric constant of the plasma sheath would decrease and increase, respectively, the influence of the plasma sheath on BRCS should be easier to be observed at lower frequencies. Hence, we repeat the scattering simulations by choosing $f = 300$ MHz. For the object flying at 7 Mach, null attack angle, and 30 km above the ground, the BRCS for both copolarizations are shown in Figure 11, in which comparisons with motionless case are also given. From Figure 11, we may conclude that the influences of the plasma sheath on the BRCS are insignificant if the object's velocity is smaller than 7 Mach and the incident wave frequency is higher than 300 MHz.

Next, we study the influences of the plasma sheath on the BRCS through the change of attack angles that can cause the asymmetry of plasma distributions. For the object flying at 10 Mach and 50 km above the ground, the comparisons for the attack angles at 0°, 5°, 10°, and 15° are shown in Figure 12, in which the incident wave frequency is again taken to be $f = 1$ GHz and the incident plane is parallel to the page ($\varphi = 0°$). The results for the incident plane perpendicular to the page ($\varphi = 90°$) are shown in Figure 13. From the graphs, we can see that the backscattering RCS are significantly changed due to the attack angles, as much as 5~15 dBm in almost all directions.

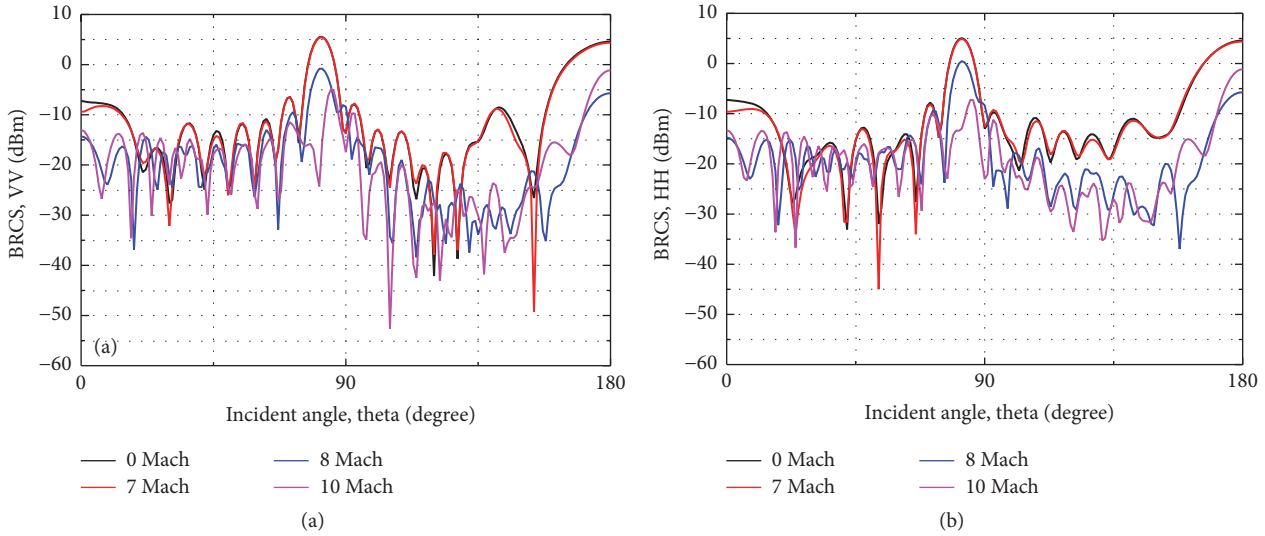

Figure 10: The influences of the plasma sheath on the backscattering RCS for the object flying at different velocities. The attack angle and height are taken to be zero degrees and 30 km above the ground. (a) For VV polarization and (b) for HH polarization.

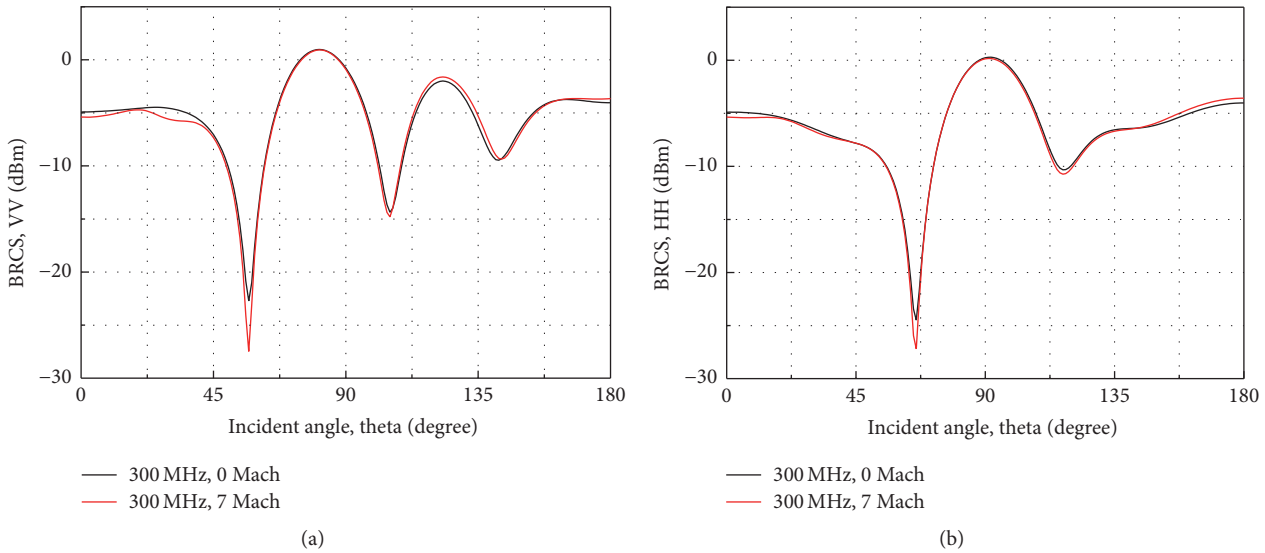

Figure 11: Comparisons of the backscattering RCS for the object velocity at 7 Mach and 0 Mach. The incident wave frequency is 300 MHz. (a) For VV polarization and (b) for HH polarization.

Finally, we consider the elevation factor that affects the formation of the plasma sheath through initial air components, temperature, and pressure. The backscattering RCS are shown in Figure 14 for the object flying at three different heights. The velocity, attack angle, and incident wave frequency are taken to be 10 Mach, zero degrees, and 1 GHz, respectively. It is seen that the backscattering RCS for the cases of 30 km and 50 km are almost identical, which are consistent with Figures 9(a) and 9(b), where the patterns of the plasma sheath look little different. The backscattering RCS for the case of 70 km is larger than that for the other two cases in most directions. This may be interpreted that the absorption is smaller because the air at 70 km high is much thinner than it is at 30 km and 50 km.

4. Concluding Remarks

A general procedure to simulate the formation of the plasma sheath and the electromagnetic scattering by a hypersonic cone-like object flying in the near space is developed. To resolve the flow fields, the Navies-Stokes equation is solved under the condition of chemical nonequilibrium, along with the Park double temperature model, and the seven species and seven reactions model. It is found that the plasma sheath is not very conspicuous if the object's velocity is smaller than 7 Mach. Radical transition seems to take place when the velocity is increased from 7 Mach to 8 Mach. The patterns of the plasma sheath look quite the same if the flight height is between 30 km and 50 km above the ground, which may be

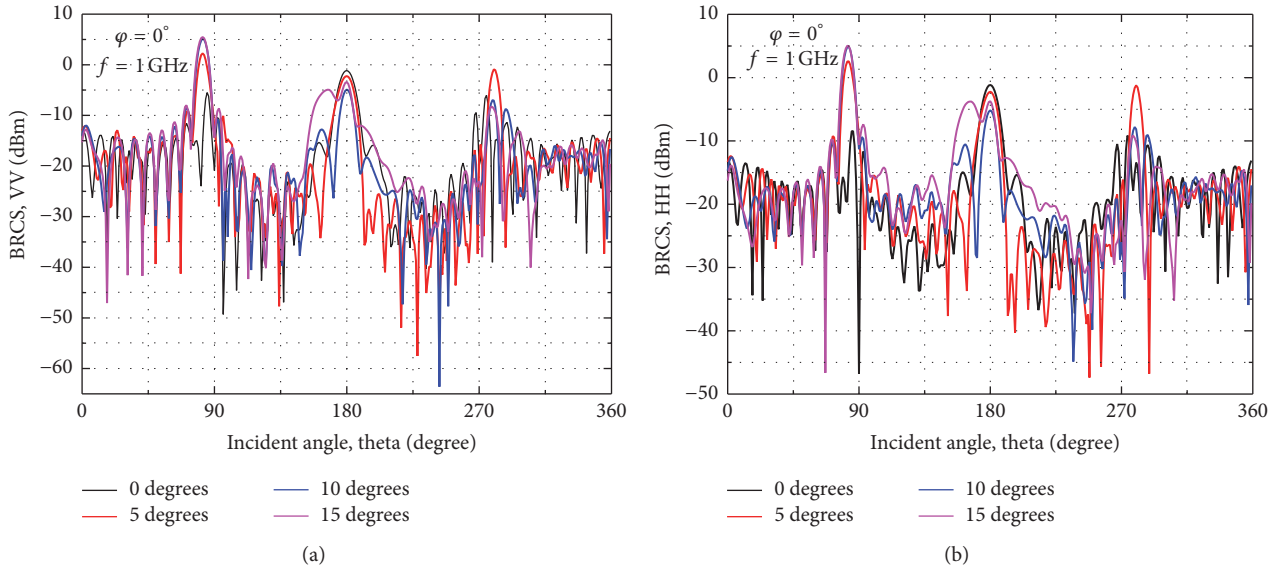

Figure 12: The backscattering RCS of the plasma sheath for the object flying at different attack angles. The velocity and height are 10 Mach and 50 km above the ground, respectively. The incident wave frequency is 1 GHz, and the incident plane is parallel to the page. (a) For VV polarization and (b) for HH polarization.

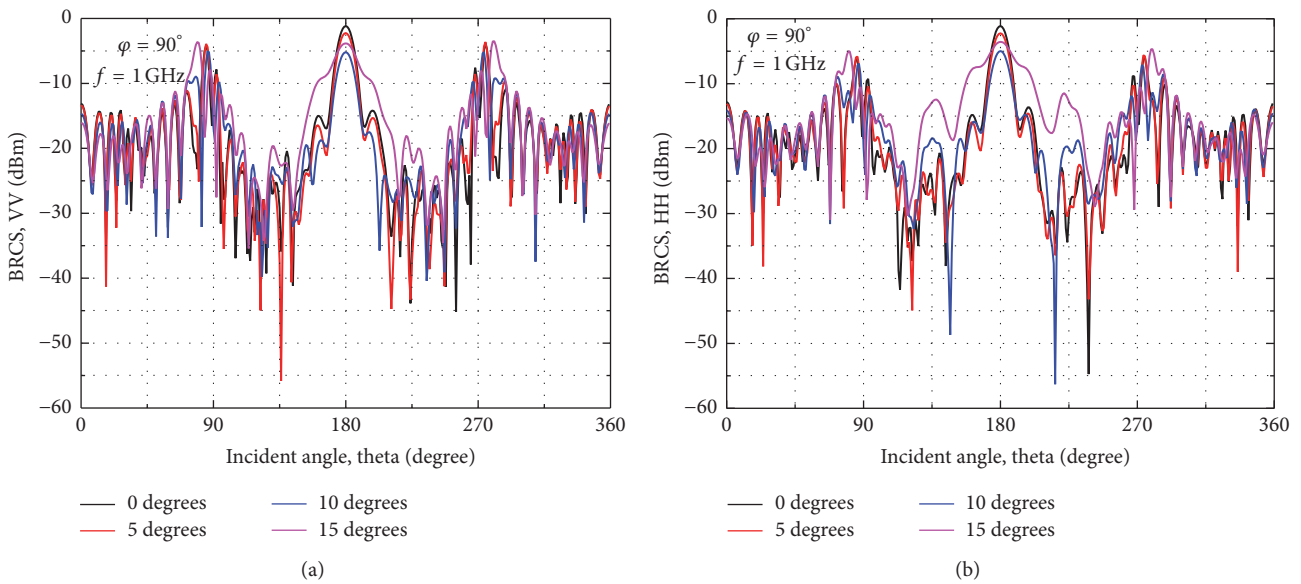

Figure 13: The backscattering RCS of the plasma sheath for the object flying at different attack angles. The velocity and height are 10 Mach and 50 km above the ground, respectively. The incident wave frequency is 1 GHz, and the incident plane is perpendicular to the page. (a) For VV polarization and (b) for HH polarization.

explained by the initial conditions that the air components, temperature, and pressure are not significantly different within the range of elevations. To extract the scattering properties of the object along with the plasma sheath, the coupled volume-surface integral equation method is employed. The multilevel fast multiple algorithm is also incorporated to accelerate the computations. Simulation results show that if the object velocity is smaller than 7 Mach, the plasma sheath effects on the Backscattering Radar Cross-Section (BRCS) would be ignorable when the incident wave frequency is higher than 300 MHz. Influences of the plasma sheath on the BRCS for the incident wave frequency at 1 GHz are subjected to radical changes as the object velocity is increased from 7 Mach to 8 Mach. In general, the BRCS would be decreased by 5~10 dBm in almost all directions because the plasma sheath would absorb some electromagnetic energy. As the velocity is continuously increased, however, the absorption seems to approach a steady level, which may be interpreted that all gas molecules are sufficiently ionized. At last, it is apparent that the present simulation results are preliminary. Further investigations on the topic are called for, including the analyses of flow fields for more realistic objects at different

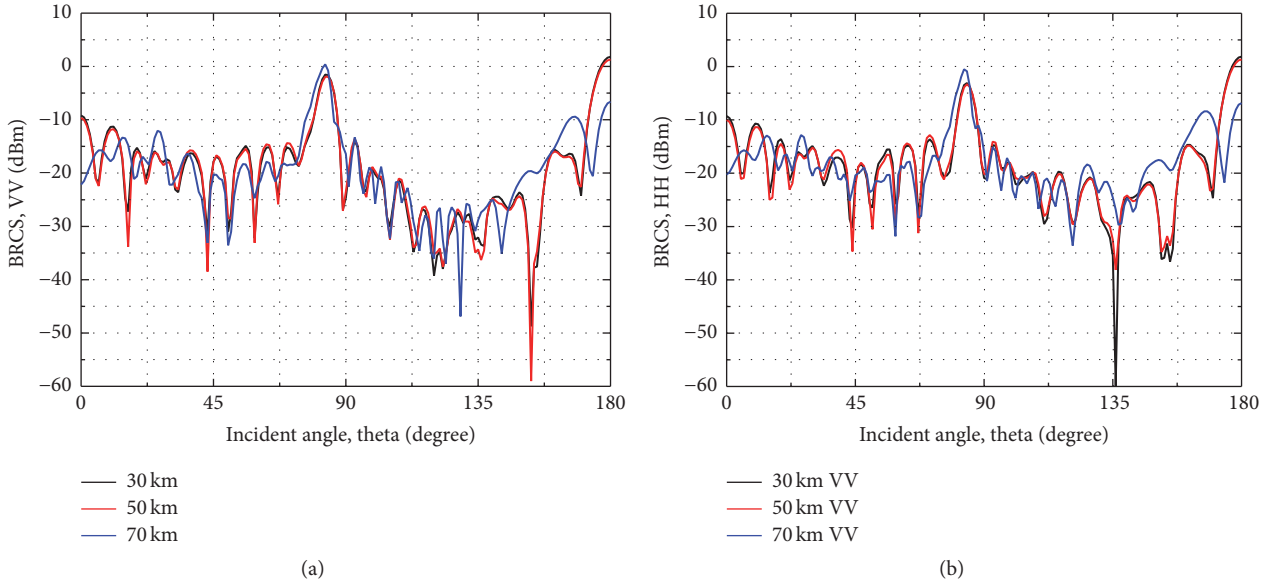

FIGURE 14: The backscattering RCS of the plasma sheath for the object flying at three different heights. The velocity, attack angle, and incident wave frequency are taken to be 10 Mach, zero degrees and 1 GHz, respectively. (a) For VV polarizations and (b) for HH polarization.

velocities and elevations and the scattering, absorbing, and penetrating properties of the plasma sheath for a range of frequencies.

Competing Interests

The authors declare that there is no conflict of interests regarding the publication of this paper.

Acknowledgments

The work is supported by the NSFC Projects 61271032 and 61531001.

References

[1] M. P. Bachynski, T. W. Johnston, and I. P. Shkarofsky, "Electromagnetic properties of high-temperature air," *IRE Transactions on Antennas and Propagation*, vol. 7, no. 5, pp. 337–339, 1959.

[2] W. B. Sisco and J. M. Fiskin, "Effect of relatively strong fields on the propagation of EM waves through a hypersonically produced plasma," *IRE Transactions on Antennas and Propagation*, vol. 7, no. 3, pp. 240–244, 1959.

[3] H. Brysk, "Electromagnetic scattering by high-density meteor trails," *IRE Transactions on Antennas and Propagation*, vol. 7, no. 5, pp. 330–336, 1959.

[4] C. Roberts, W. Sisco, and J. Fiskin, "Theory of equilibrium electron and particle densities behind normal and oblique hypersonic shock waves in air," *IRE Transactions on Antennas and Propagation*, vol. 8, no. 1, pp. 102–103, 1960.

[5] L. Lees, "Hypersonic wakes and trails," *AIAA Journal*, vol. 2, no. 3, pp. 417–428, 1964.

[6] T. H. Lee, "Backscattering of electromagnetic waves by inhomogeneous plasma wakes," *IEEE Antennas and Propagation Society International Symposium*, vol. 1, pp. 190–192, 1963.

[7] R. D. Kodis, "The scattering cross section of a composite cylinder, geometric optics," *Institute of Electrical and Electronics Engineers. Transactions on Antennas and Propagation*, vol. 11, no. 1, pp. 86–93, 1963.

[8] F. H. Mitchell, W. R. Mahaffey, and R. F. Jacob, "Modeling plasma effects on radar cross section of reentry vehicles," *IBM Journal of Research and Development*, vol. 13, no. 4, pp. 468–474, 1969.

[9] C. M. deRidder and S. Edelberg, "Scattering from a rapially varying plasma cylinder of infinite length," MIT Lincoln Laboratory 312G-8, 1962.

[10] H. C. Chen and D. K. Cheng, "Scattering of electromagnetic waves by an anisotropic plasma-coated conducting cylinder,," *IEEE Transactions on Antennas and Propagation*, vol. 12, no. 3, pp. 348–353, 1964.

[11] W. V. T. Rusch and C. Yeh, "Scattering by an infinite cylinder coated with an inhomogeneous and anisotropic plasma sheath," *IEEE Transactions on Antennas and Propagation*, vol. 15, no. 3, pp. 452–457, 1967.

[12] K. Fong, "Computation of backscattering cross section of plasma-clad metal cylinders by the 'layer method'," *IEEE Transactions on Antennas and Propagation*, vol. 16, no. 1, pp. 138–140, 1968.

[13] R. D. Kodis, "Propagation and scattering in plasmas," *Proceedings of the IEEE*, vol. 53, no. 8, pp. 1016–1024, 1965.

[14] J. P. Rybak and R. J. Churchill, "Progress in reentry communications," *IEEE Transactions on Aerospace and Electronic Systems*, vol. 7, no. 5, pp. 879–894, 1971.

[15] R. Dutta, R. Biswas, and N. Roy, "Reduction of attenuation of e.m wave inside plasma formed during supersonic or hypersonic re-entry of missile like flight vehicles by the application of D.C magnetic field—a technique for mitigation of RF Blackout," in *Proceedings of the IEEE Applied Electromagnetics Conference (AEMC '11)*, IEEE, Kolkata, India, December 2011.

[16] G.-X. Fan and Q. H. Liu, "An FDTD algorithm with perfectly matched layers for general dispersive media," *IEEE Transactions on Antennas and Propagation*, vol. 48, no. 5, pp. 637–646, 2000.

[17] B. Chaudhury and S. Chaturvedi, "Three-dimensional computation of reduction in radar cross section using plasma shielding," *IEEE Transactions on Plasma Science*, vol. 33, no. 6, pp. 2027–2034, 2005.

[18] B. Chaudhury and S. Chaturvedi, "Study and optimization of plasma-based radar cross section reduction using three-dimensional computations," *IEEE Transactions on Plasma Science*, vol. 37, no. 11, pp. 2116–2127, 2009.

[19] X.-J. Zeng, Z.-F. Yu, S.-Q. Bu et al., "Research on the RCS of hypervelocity model and its plasma sheath," *Acta Aerodynamica Sinica*, vol. 28, no. 6, pp. 645–649, 2010.

[20] L. Lei, J. Hu, and H.-Q. Hu, "Solving scattering from conducting body coated by thin-layer material by hybrid shell vector element with boundary integral method," *International Journal of Antennas and Propagation*, vol. 2012, Article ID 854647, 7 pages, 2012.

[21] C. C. Lu and W. C. Chew, "Electromagnetic scattering from material coated PEC objects: a hybrid volume and surface integral equation approach," in *Proceedings of the IEEE Antennas and Propagation Society International Symposium*, vol. 4, pp. 2562–2565, Orlando, Fla, USA, 1999.

[22] Z. Zeng and C.-C. Lu, "Discretization of hybrid VSIE using mixed mesh elements with zeroth-order galerkin basis functions," *IEEE Transactions on Antennas and Propagation*, vol. 54, no. 6, pp. 1863–1870, 2006.

[23] L. J. Gomez, A. C. Yücel, and E. Michielssen, "Volume-surface combined field integral equation for plasma scatterers," *IEEE Antennas and Wireless Propagation Letters*, vol. 14, pp. 1064–1067, 2015.

[24] I.-T. Chiang and W. C. Chew, "A coupled PEC-TDS surface integral equation approach for electromagnetic scattering and radiation from composite metallic and thin dielectric objects," *IEEE Transactions on Antennas and Propagation*, vol. 54, no. 11, pp. 3511–3516, 2006.

[25] X. Niu, Z. Nie, X. Que, and S. He, "Modified multi-layer TDS approximation for dielectric-coated targets," in *Proceedings of the IEEE Antennas and Propagation Society International Symposium (APSURSI '13)*, pp. 742–743, Orlando, Fla, USA, July 2013.

[26] J. D. Anderson, *Hypersonic and High Temperature Gas Dynamics*, McGraw-Hill, New York, NY, USA, 1989.

[27] C. Park, "Assessment of two-temperature kinetic model for ionizing air," *Journal of Thermophysics and Heat Transfer*, vol. 3, no. 3, pp. 233–244, 1989.

[28] E. W. Miner and C. H. Lewis, "Hypersonic ionizing air viscous shock-layer flows over nonanalytic blunt bodies," NASA Technical Report, 1975.

[29] J.-T. Li, L.-X. Guo, S.-S. Jin, and Q.-J. Fang, "EM wave propagation characteristic in plasma sheath," *Chinese Journal of Radio Science*, vol. 26, no. 3, pp. 494–499, 2011.

[30] D. H. Schaubert, D. H. Schaubert, D. R. Wilton, D. R. Wilton, and A. W. Glisson, "A tetrahedral modeling method for electromagnetic scattering by arbitrarily shaped inhomogeneous dielectric bodies," *IEEE Transactions on Antennas and Propagation*, vol. 32, no. 1, pp. 77–85, 1984.

[31] S. M. Rao, D. R. Wilton, and A. W. Glisson, "Electromagnetic scattering by surfaces of arbitrary shape," *IEEE Transactions on Antennas and Propagation*, vol. 30, no. 3, pp. 409–418, 1982.

[32] W. L. Jones and A. E. Cross, *Electrostatic-Probe Measurements of Plasma Parameters for Two Reentry Flight Experiments at 25000 Feet per Second*, NASA Langley Research Center, 1972.